17th Australasian Wind Engineering Society Workshop
Wellington, New Zealand
12-13 February 2015

Wind Turbine Siting on Rugged Cliffs

J. Rowcroft[1], D. Burton[1], H.M. Blackburn[1] and J. Sheridan[1]

[1]Department of Mechanical and Aerospace Engineering
Monash University, Victoria 3800, Australia

Abstract

Wind farms in Australia are often located in the vicinity of coastal cliffs, taking advantage of coastal winds and the speed-up associated with flow over cliffs. Erosion causes lateral variations to otherwise straight-edged cliffs. The flow topology associated with these different shaped lateral variations has been determined with wind tunnel investigations. Wind speed and turbulence statistics have also been examined. Comparisons are made with the flow structure associated with delta wings, in particular, the bursting phenomenon.

Introduction

To ensure wind energy is cost-competitive, wind turbines need to be located in regions of high mean wind speed, whilst minimising loading on the turbines that result in increased maintenance costs. Coastal regions are typically associated with consistent strong winds. Cliffs or forward facing steps (FFSs) are associated with further increases in wind speed (Bowen and Lindley, 1975).

While it is well established that FFSs generate regions of accelerated flow downstream of their crests (Bowen and Lindley, 1977; Rowcroft et al., 2013; Sherry et al., 2010), the natural variations associated with this type of geometry have not been extensively examined, with the exception of the work of Cochard et al. (2012) and Montlaur et al. (2012) who completed complementary wind tunnel and computational studies of flow over FFSs with sawtooth lateral variations. They identified delta wing-style vortices forming from the tip of the sawtooth element. Whilst there was undoubtedly a region above the sawtooth element with increased wind speed and negligible change to turbulence intensity (TI), it was observed that in cases where the wind direction did not coincide with the x-direction, as shown in Figure 1, the leading vortex would increase in diameter, resulting in a large region of increased TI and reduced wind speed. Thus, unless wind direction would remain constant in the x-direction, the sawtooth elements would be unsuitable locations for the siting of wind turbines.

The research presented here extends the work of Cochard et al. (2012) and Montlaur et al. (2012) by varying the amplitude to wave length ratio (A/λ) of the sawtooth, as shown in Figure 1. In addition, the sawtooth FFSs are compared to sinusoidal FFSs with corresponding A/λ values. The flow topology, in each case, is derived using paint droplet visualisation. For the lowest A/λ cases, four-hole pressure probe (Cobra Probe) measurements are used to evaluate the flow fields.

Methodology

This research was conducted in the Monash University 450 kW wind tunnel. Experiments were performed at a fan blade pitch angle of 30°, corresponding to a free-stream speed of 34 ms^{-1}, over forward facing steps of height, $h = 0.050$ m. The experiments were completed at Reynolds Numbers of 1×10^5, using the step height, h, as the reference length. End plates extended 12h upstream of the models. The models resulted in 2.5% blockage and extended beyond 10h downstream, and can be thus considered isolated cliffs according to Moss and Baker (1980). The aspect ratio was 34, resulting in four complete periods of the sawtooth or sinusoid geometry. The models were painted with semi-gloss enamel paint, and were aerodynamically smooth. The experimental domain is presented in Figure 1, while the geometric parameters are presented in Table 1.

The inflow configuration was developed over a false floor, with a fetch of 32h. All Cobra Probe measurements were conducted at a frequency of 5000 Hz and down-sampled to 2500 Hz. The sample length was 180 s. The free-stream TI was 1% and the boundary layer thickness was 0.100 m. The integral length scale was calculated by fitting the von Kármán equation to the power spectral density. The velocity, TI and stream-wise integral length scale profiles are presented in Figure 2 and Figure 3. The resulting boundary layer thickness to step height ratio, δ/h, was 2.

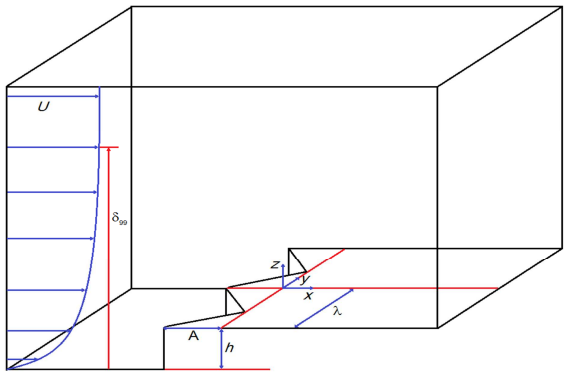

Figure 1. Experimental domain for FFS with sawtooth lateral variation.

The paint droplet visualisation technique was used to depict the surface shear stress vector field, giving an indication of the strength of the surface shear stress, but more importantly, the direction in which it acts. This technique is an adaptation of traditional oil film visualisations. Here, an initial group of droplets is deposited on the model surface with a hypodermic syringe in such a way as to avoid the streaks from overlapping when the wind is applied. Additional droplets are then applied in the same manner, and the process repeated until the flow field can be described. The paint used was a magenta-coloured water-based paint diluted with tap water to approximately a 1:1 ratio to provide a paint mixture with a viscosity such that the droplets would streak freely across the surface but not speckle when subjected to the wind tunnel flow. Obtaining this ideal viscosity required some trial and error. Each droplet was approximately 0.1 mL. The process is shown in Figure 4.

h	A/λ	A	λ	Extent downstream	Aspect ratio
0.05 m	0.325	0.130 m	0.400 m	2.6 m/52h	34
0.05 m	0.5	0.200 m	0.400 m	2.6 m/52h	34
0.05 m	0.6625	0.265 m	0.400 m	2.6 m/52h	34
0.05 m	1	0.400 m	0.400 m	2.6 m/52h	34

Table 1. Geometric configurations tested for both sawtooth and sinusoidal cases.

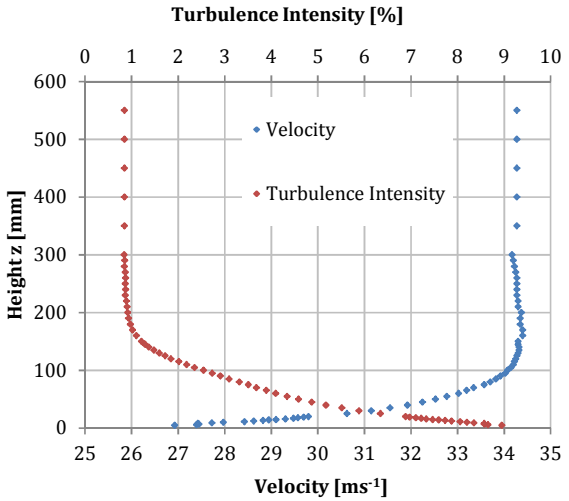

Figure 2. Inflow wind speed and TI.

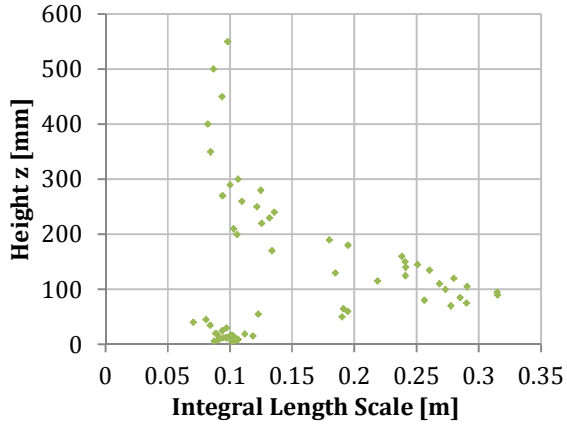

Figure 3. Inflow integral length scale, based on von Kármán equation.

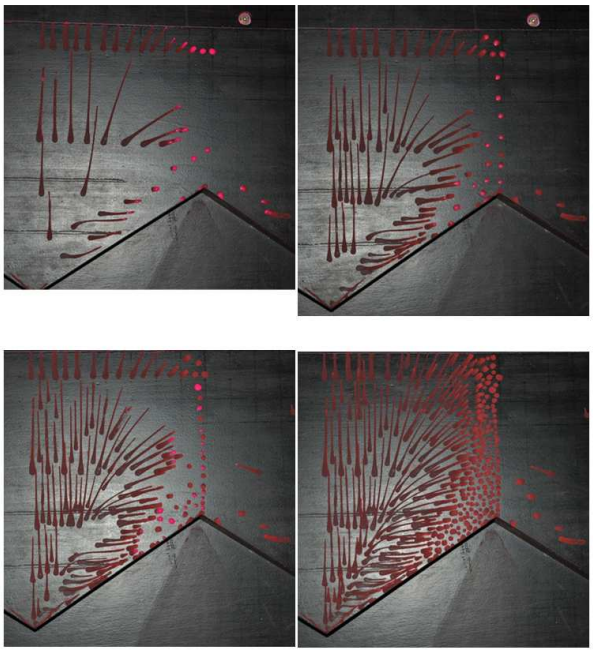

Figure 4. Demonstration of build-up technique. Four instances are shown. Intermediate steps are omitted for brevity.

Results and Discussion

The paint droplet visualisations for the sawtooth geometries are presented in Figure 5. From these visualisations, the flow topology associated with each case can be determined using critical point theory and the Poincaré-Bendixson Theorem (Perry and Chong, 1987). These are presented in Figure 6.

The corresponding visualisations and flow topologies for the sinusoidal cases are presented in Figure 7 and Figure 8.

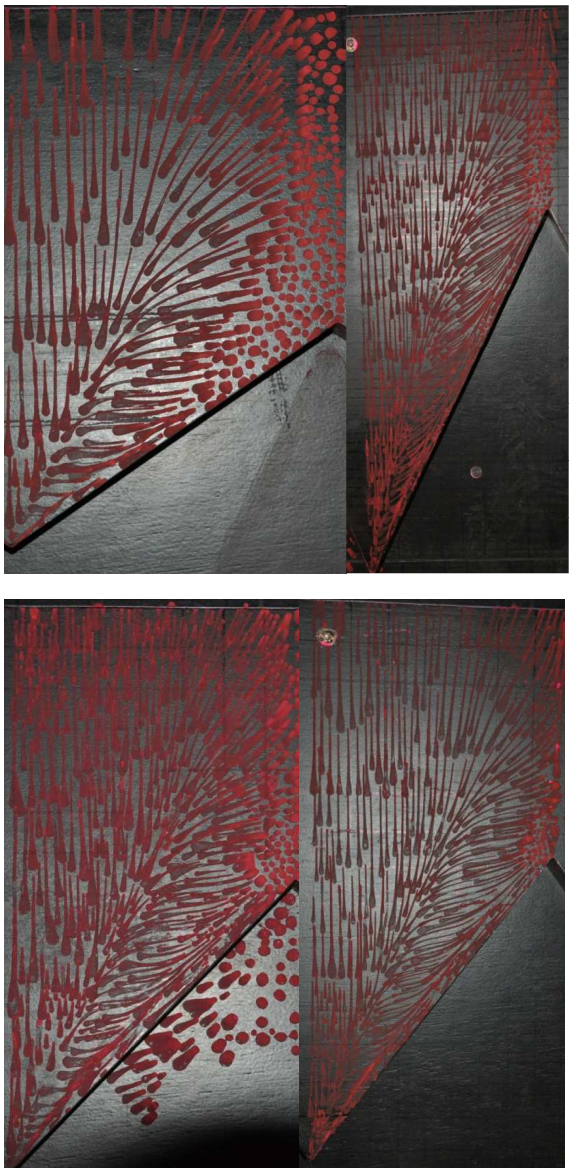

Figure 5. Paint droplet visualisations. In each pane, flow is from bottom to top. Top left: $A/\lambda = 0.325$. Top right: $A/\lambda = 1$. Bottom left: $A/\lambda = 0.5$. Bottom right: $A/\lambda = 0.6625$.

The flow topology over each of the sawtooth and sinusoidal cases is in good agreement with the flow structure described by Cochard et al. (2012) and Montlaur et al. (2012), with respect to the development of delta wing style vortices being generated.

The topological development of the sawtooth cases is considered first. These are presented in Figure 6. In the shallowest case ($A/\lambda = 0.325$), the primary vortex structure separates from the crest. Increases to A/λ result in the primary vortex remaining

attached to the length of the crest, and the secondary structures becoming more important in determining the flow topology.

The topology observed experimentally in the $A/\lambda = 0.65$ case was shown to be equivalent to the $A/\lambda = 0.5$ case, and strictly speaking, to the $A/\lambda = 0.325$ case. A distinction is made between the $A/\lambda = 0.325$ case and the other two cases because of the attachment of the primary vortex along the crest through to the trough region, and the secondary structures that feed into the stable node.

The $A/\lambda = 1$ case is the steepest of the models. Its mean topology indicates that pairs of counter rotating vortices rise from the surface in a stable manner and become entwined with the primary vortex. This case is distinct from the others.

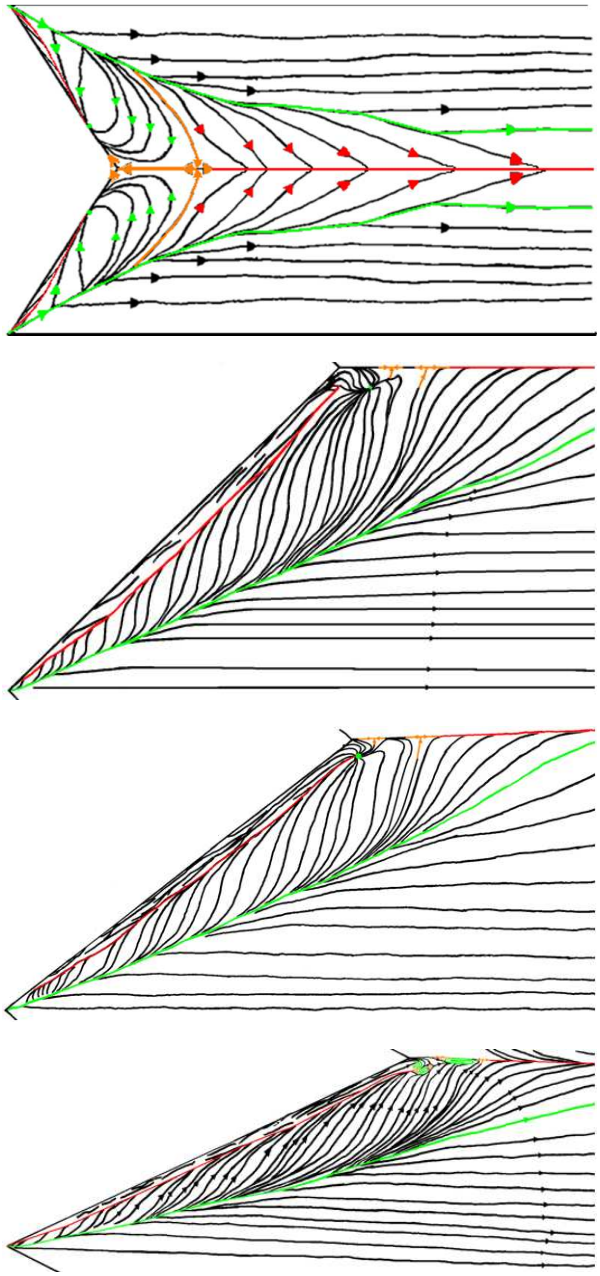

Figure 6. Flow topology derived from paint droplet visualisation on sawtooth cases. From top to bottom, $A/\lambda = 0.325$, 0.5, 0.6625, 1.

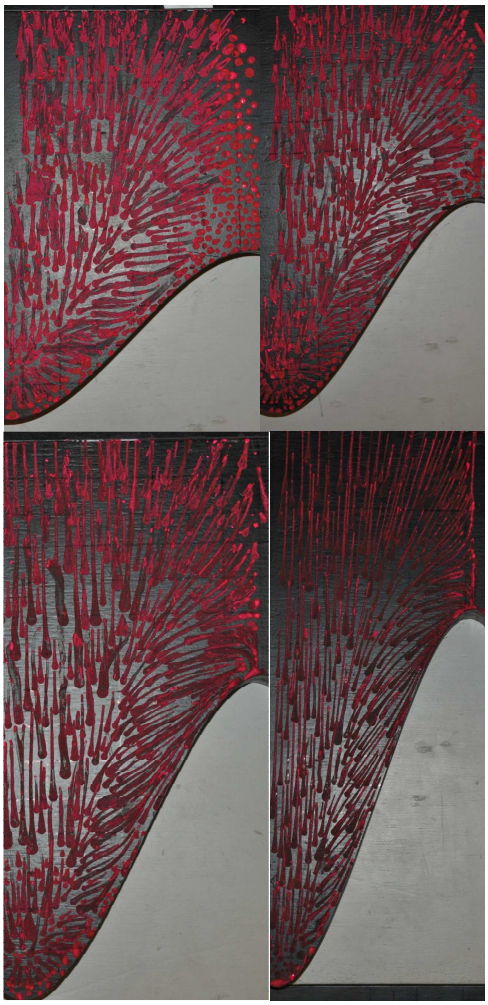

Figure 7. Paint droplet visualisations. In each pane, flow is from bottom to top. Top left: $A/\lambda = 0.325$. Top right: $A/\lambda = 0.5$. Bottom left: $A/\lambda = 0.6625$. Bottom right: $A/\lambda = 1$.

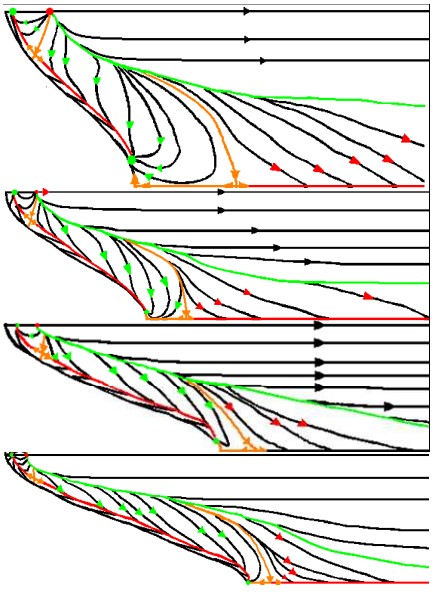

Figure 8. Flow topology derived from paint droplet visualisation on sinusoidal cases. From top to bottom, $A/\lambda = 0.325$, 0.5, 0.6625, 1.

For the sinusoidal FFS cases, topological equivalence is maintained through the range of A/λ investigated, which can be attributed to the curvature of the crest. The flow structure features a recirculation region over the peak protrusion of the sinusoid which propagates downstream along the crest of the cliff, generating a delta wing style vortex structure. The vortex separates from the crest of the step and persists downstream into the far wake. In the topological development shown in Figure 8, the separation point approaches the trough point as A/λ increased. In the sawtooth cases it was only the A/λ = 0.325 case where separation occurred part way along the crest.

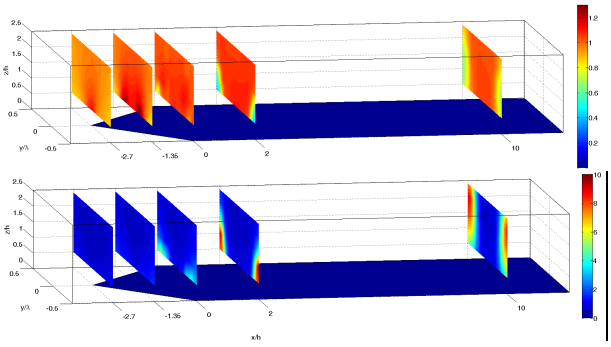

Figure 9. Cobra Probe measurements over A/λ = 0.325 sawtooth case. Fractional speed up ratio (Top) and TI ratio (Bottom) are presented.

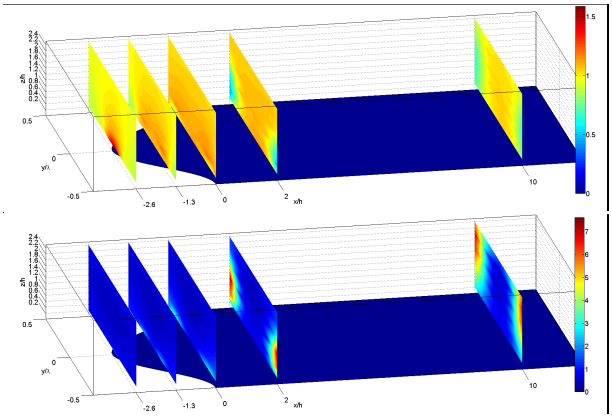

Figure 10. Cobra Probe measurements over A/λ = 0.325 sinusoidal case. Fractional speed up ratio (Top) and TI ratio (Bottom) are presented.

Cobra Probe measurements are presented in Figure 9 and Figure 10 for the A/λ = 0.325 sawtooth and sinusoidal cases respectively. Fractional speed up ratio is defined in Equation (1) and TI ratio is defined in Equation (2).

$$S = \frac{U_{Model}(x,z) / U_{Pitot,Model}}{U_{BL}(z) / U_{Pitot,BL}} \quad (1)$$

$U_{Model}(x,z)$ is the velocity at a point (x,z), according to the previously defined Cartesian co-ordinate system. $U_{Pitot,\ Model}$ is the velocity measured at the up-stream Pitot-Static tube, measured concurrently to $U_{Model}(x,z)$. $U_{BL}(z)$ is the velocity in the undisturbed boundary layer, that is, without the model in place, at $x = 0$. $U_{Pitot,\ BL}$ is the velocity measured at the up-stream Pitot-Static tube, measured concurrently to $U_{BL}(z)$.

$$TI\ Ratio = \frac{I_{uvw,Model}(x,z)}{I_{uvw,BL}(z)} \quad (2)$$

$I_{uvw}(x,z)$ is the TI based on the three velocity components, with the *Model* and *BL* subscripts, and the (x,z) location having the same meaning as in Equation (1).

These plots provide a layer of validation for the flow structures that have been derived based on the paint droplet visualisations. Furthermore, they give an idea of the vertical scale associated with the vortex development at both the crest and 10*h* downstream. Over the sawtooth and sinusoidal protrusions, increases in wind speed (fractional speed up greater than unity) and negligible variation in fractional change in TI are observed. However, diffusion of the vortex structure occurs from the trough point ($x/h = 0$) through to the far wake, as evidenced by the increased TI and decrease in flow speed. This expansion and stagnation is identified as vortex bursting (Hall, 1972).

Conclusions

Topological analyses of flow over FFSs with sawtooth and sinusoidal lateral variation highlight regions where vortex structures exist. Cobra Probe data exhibited evidence of vortex bursting. It is essential to avoid siting wind turbines where their blades will pass through vortex structures – whether or not they have burst. Prior to bursting, the delta wing vortex structures induce large shear on wind turbine rotors, resulting in unbalanced rotor loads. Post bursting, the vortex structures are associated with low wind speeds and high TI. To take advantage of the increased wind speeds associated with such topographies, siting turbines such that the blade tip passes above the unburst vortex may be a solution.

Acknowledgements

The authors would like to recognise Monash University, Hydro Tasmania and Suzlon Australia for their financial support of this work; and Don McMaster for his technical assistance. This research was supported under the Australian Research Council's Linkage Project funding scheme, project number LP100100746.

References

Bowen A J, and Lindley D (1977) A wind tunnel investigation of the wind speed and turbulence characteristics close to the ground over various shaped escarpments, Boundary Layer Meterology 12: 259-271

Cochard S, Letchford C W, Earl T A, and Montlaur A (2012) Formation of tip-vortices on triangular prismatic-shaped cliffs Part 1: A wind tunnel study Journal of Wind Engineering and Industrial Aerodynamics, 109, 9-20

Hall M G (1972) Vortex Breakdown, Annual Review of Fluid Mechanics 4: 195-218

Montlaur A, Cochard S, and Fletcher D F (2012) Formation of tip-vortices on triangular prismatic-shaped cliffs Part 2: A computational fluid dynamics study, Journal of Wind Engineering and Industrial Aerodynamics 109: 21-30

Moss W, and Baker S (1980) Re-circulating flows associated with two-dimensional steps, Aeronautical Quarterly 31(August): 151-172

Perry A E, and Chong M S (1987) A description of eddying motions and flow patterns using critical-point concepts, Annual Review of Fluid Mechanics 19: 125-155

Rowcroft J, Burton D, Blackburn H M, and Sheridan J (2013) Optimal Placement of Wind Turbines on Cliffs Paper, presented at the 16th Australasian Wind Engineering Society Workshop, Brisbane

Sherry M, Lo Jacono D, and Sheridan J (2010) An experimental investigation of the recirculation zone formed downstream of a forward facing step, Journal of Wind Engineering and Industrial Aerodynamics 98(12): 888-894.